H.Y. RYU*, S.C. KWON*, M.H. HAN*, Y.S. AN***, J.S. LEE***, J.H. LEE *,**,♯

MORPHOLOGY CHANGE OF Si DEPOSIT IN MOLTEN SALT ELECTROREFINING

ZMIANA MORFOLOGII OSADU Si PODCZAS ELEKTRORAFINACJI W STOPIONYCH SOLACH

The effects of processing parameters on the morphology change in a Si deposit recovered by means of molten salt electrorefining are evaluated using electrochemical techniques such as cyclic voltammetry and chronopotentiometry at 800°C. It was found that concentration of K_2SiF_6 and current density were important parameters in determining deposit size. Higher concentrations of K_2SiF_6 were effective in coarsening the silicon deposit and decreasing the cell potential. Silicon nanofiber was recovered at 5 wt% of K_2SiF_6 whereas dense particles were prepared at 30 and 50 wt% of K_2SiF_6. The morphology of the Si deposit was determined by the concentration of Si in the electrolyte which is related to the formation of crystal and growth of Si. The formation mechanism of the Si deposit was interpreted by using high resolution TEM as well as electrochemical properties.

Keywords: Molten salt, Silicon, Morphology, Electrorefining, Current density

1. Introduction

Silicon materials are widely used in semiconductors for photovoltaic and electronic devices. Another promising application of silicon has arisen in the field of secondary battery cathodes and there have been increasing interest in this area. Ultra high purity silicon has been used for semiconductor grades ranging from 6N to 11N while the morphology of silicon with a nanofibrous shape and moderate purity exhibits superior characteristics when it is used for cathode material of secondary batteries [1-3]. There are a number of processes for preparing silicon nanofiber, and the processes are classified into two large groups, electrospinning [4] and etching of bulk silicon [3]. Recently we reported that silicon nanofiber could be prepared using an electrorefining process in molten salt media [5]. The process recovers high purity fiber from metallurgical grade silicon via chemical separation of impurities using an intrinsic property of the electrorefining process. The shape of a deposit of silicon is important according to the application. When the purpose of the electrorefining is to recover a high purity product, the cathode deposit is coarse with high density due to minimized surface oxidation and incorporation of an electrolyte containing impurities [6,7]. In particular, the grain boundary is an important structural place where impurities are segregated [8]. This means that controlling the microstructure of a cathode deposit is a key factor in the molten salt electrorefining process not only for purification of feedstocks but also for synthesis of functional material like nanofibers. In spite of the importance, research on morphology control is rare. Hence, in this study, we investigated the effects of the processing parameters on the morphology change of the silicon cathode deposit.

2. Experimental

Si lump (purity <98%, size >20 mm, Daejung Chemical and Metals Co., Ltd., South Korea) and LiF, KF (99% pure, Daejung Chemical and Metals Co., Ltd., South Korea) , and K_2SiF_6 (99% pure, Junsei Chemical Co., Ltd., Japan) salts were used as starting materials for electrorefining MG-silicon.

For cyclic voltammetry (CV), a platinum wire with a diameter of 0.3 mm was used both as a reference electrode and counter electrode with a plate with the dimensions $10 \times 0.3 \times 50$ mm. Molybdenum wire with diameter of 0.5 mm was used as a working electrode as shown Fig. 1 (a). Fresh molybdenum wire forms $MoSi_2$ during a CV experiment in such a high temperature molten salt environment that it is not appropriate as a stable electrode, but after the formation of a $MoSi_2$ phase, it becomes an intact cathode material that suitable for electrodeposition of silicon [5]. Fig. 1 (b) shows the electrorefining cell with a silver cathode with the dimensions $10 \times 1 \times 100$ mm, Fig. 1 (c), and a 20 g MG-Si lump as shown in Fig. 1 (d). The reference electrode was a Pt wire with a diameter of 0.3 mm. A LiF-KF eutectic system (51-49 mol%; T_m, 492°C) and K_2SiF_6 were handled in a glove box where both the oxygen and the moisture content in an argon atmosphere were maintained below 2 ppm. The temperature was maintained

*   GRADUATE SCHOOL OF ENERGY SCIENCE AND TECHNOLOGY
**   DEPARTMENT OF NANOMATERIALS ENGINEERING, CHUNGNAM NATIONAL UNIVERSITY, 79 DAEHAK-RO, YUSEONG-GU, 305-764, DAEJEON, REPUBLIC OF KOREA
***   ENERGY MATERIALS CENTER, KOREA INSTITUTE OF ENERGY RESEARCH, 152 GAJEONG-RO, YUSEONG-GU, 305-343, DAEJEON, REPUBLIC OF KOREA
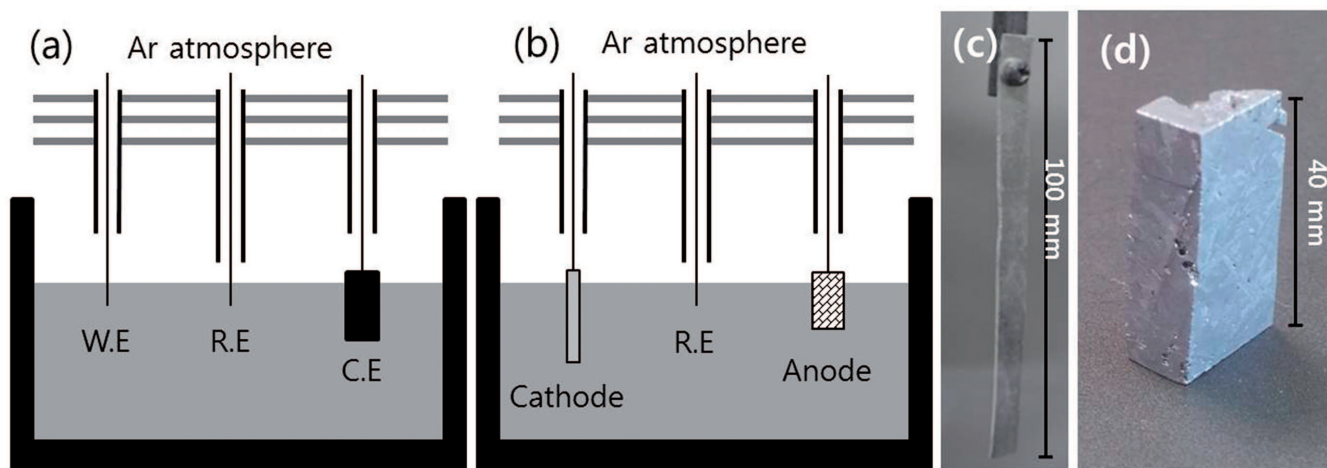♯   Corresponding author: jonglee@cnu.ac.kr

Fig. 1. Three electrode electrochemical cell used for cyclic voltammetry (a) and electrorefining of silicon (b), (c) and (d) show silver cathode and MG-Si anode for electrorefining respectively. (working electrode(W.E): molybdenum, reference electrode(R.E): platinum, counter electrode(C.E): platinum)
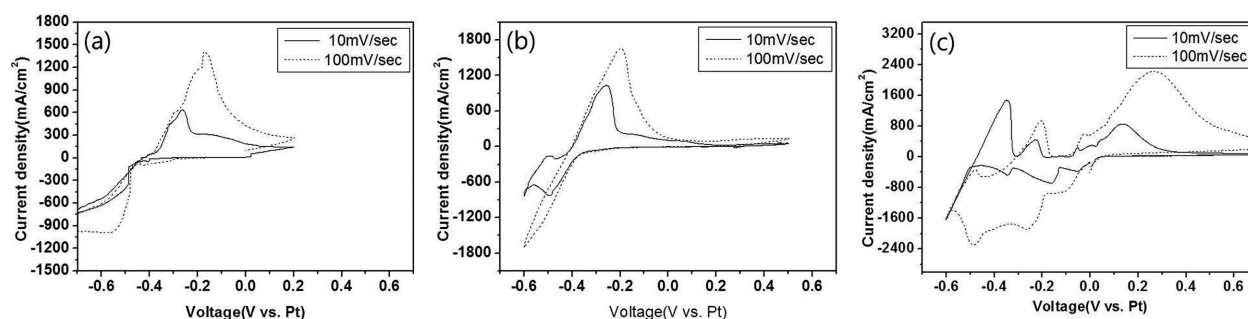

Fig. 2. Cyclic voltammograms at various K_2SiF_6 concentrations in the LiF-KF-xK_2SiF_6 system at 800°C: (a) 5 wt%, (b) 30 wt%, (c) 50 wt%

at 800°C, and the electrode potential and current were controlled using a WonATech potentiostat. The electrorefined Si deposit on the Ag cathode was leached with warm distilled water containing 3% HCl and washed 3 times.

The deposit morphology was examined using a scanning electron microscope (SEM; JSM 5410, JEOL, Japan) and transmission electron microscopes (TEM; Tecnai G2 F30, FEI, USA). The deposit size was analyzed using a particle size analyzer (NANOPHOX, Sympatec GmbH, Germany). The phases were identified by X-ray diffraction (XRD, Siemens D5000, Germany) measurement.

3. Results and discussion

3.1. Comparison of cyclic voltammetry between inert and consumable electrodes

The reduction potential of Si was confirmed by cyclic voltammetry as shown in Fig. 2. Figure 2 (a) shows the potential and current response of the eutectic LiF-KF electrolyte with 5 wt% K_2SiF_6. There is some controversy over the mechanism by which fluorosilicate is reduced. It is contested whether this occurs by the double-step reduction of Si(IV) via Si(II) [9] or the single-step reduction of Si(IV) [10]. Here, we were able to clearly measure two cathodic peaks with cyclic voltammetry, as shown in Fig. 2 (a), and found that the peak currents increased with the scanning rate. This result confirms

that Si(IV) is reduced by double-step reduction as reported by R. Boen. There was a plateau until -0.1V (vs. Pt) and gradual decrease to -0.4 V showing a reduction peak of Si as the K_2SiF_6 concentration increased to 30 wt% as shown in Fig. 2 (b). Figure 2 (c) shows different CV behavior from the other data obtained below 30 wt% of K_2SiF_6 concentration. The first reduction peak appeared at 0.05V (vs. Pt) with 50 wt% of K_2SiF_6 concentration and the slope of the first peak drastically increased compared to that at a lower concentration. Peak currents also increased from 400 mA/cm^2 to 950 mA/cm^2 as the scan rate increased from 10 mV/sec to 100 mV/sec. There were two more peaks that were not observed until 30 wt% of K_2SiF_6 concentration at -0.15 V (vs. Pt) and -0.3 V (vs.Pt). It seems that the reduction mechanism of Si(IV) changes from the direct reduction of Si(IV)→Si(0) to a multi step reduction through a lower balance state such as Si(III), Si(II) and Si(I). The other reduction peak at -0.5 V is related to the reduction of potassium. Potassium is supposed to be reduced at a much lower reduction potential than -0.5 V, but potassium could be reduced at such a high potential because of the high vapor pressure of potassium at the electrolysis temperature of 800°C in this study as reported by G. J. Kipouros [11]. Silicon also easily forms intermetallic compounds such as KSi, $K_{12}Si_{17}$, K_8Si_{46}, K_7Si_{46} with potassium [12], which leads to reduction of silicon at a more positive potential than its standard potential, the so-called under potential deposition. The other possible explanation is that potassium could be more easily

reduced as the concentration of KF increased as K_2SiF_6 was decomposed into KF and SiF_4.

3.2. Polarization behavior according to concentration of K_2SiF_6

To investigate polarization behavior, constant currents were applied to the cell with the MG-Si anode and Ag cathode with well-measured surface areas for 2 min at each current level at various concentrations of K_2SiF_6 at 800°C, as shown in Fig. 3. The conductivities of the anode and cathode were respectively 216.83 mS/cm^2 and 94.34 mS/cm^2 at 5 wt% of K_2SiF_6 and the conductivity of the cathode drastically increased to 2500 mS/cm^2 with an increase in the concentration of K_2SiF_6 to 30 wt%. This is because the concentration overpotential decreased by increasing the ion concentration of silicon in the molten salt. There was no change in the conductivity of the cathode as the concentration of K_2SiF_6 increased from 30 wt% to 50 wt%, which means that sufficient diffusion took place in the vicinity of the boundary layer on the cathode surface with more than 30 wt% of K_2SiF_6 concentration. In the anode, the conductivity increased from 161.6 mS/cm^2 to 182.3 mS/cm^2 which is negligible compared to that of the cathode. Concentration increases of K_2SiF_6 also moved the redoxpotential of the silicon to the positive side because of an increase in the activity silicon ions as the K_2SiF_6 concentration increased.
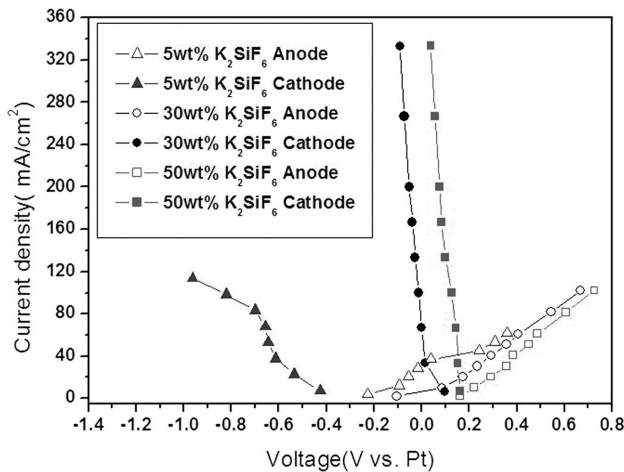

Fig. 3. Polarization behavior in MG-Si electrorefining system at various K_2SiF_6 concentrations in LiF-KF-xK_2SiF_6 system at 800°C

We previously reported that silicon nano fiber was formed by electrolysis in a LiF-KF-5 wt% K_2SiF_6 molten salt system at 700°C [5]. A series of experiments was conducted at 800°C in the same electrolyte system and chronopotentiometry and voltage variations as shown in Fig. 4 with 40 mA/cm^2 for 5 hrs. The cathode potential started from -0.1 V (vs. Pt) and immediately decreased after that and finally it was maintained at -0.9 V (vs. Pt) after 1 hr of the onset of electrodeposition. The anode potential started from 0.3 V (vs. Pt) and was then maintained as 0.15 V (vs. Pt) after 1 hr. The cell voltage started from 0.4 V and was then maintained at a constant value of 1.15 V after 1 hr, which means equilibrium between deposition and dissolution of silicon was leached at that time.
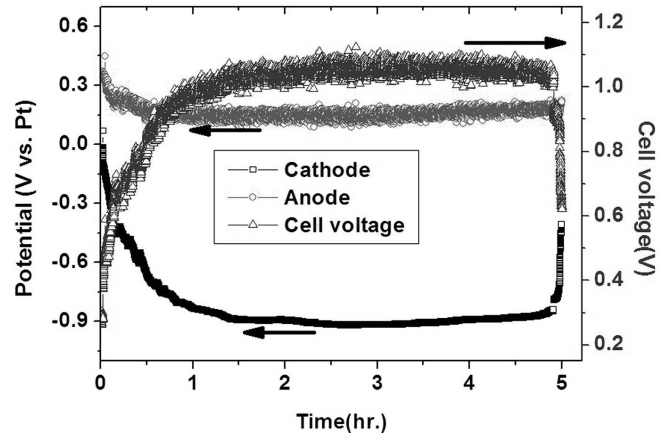

Fig. 4. Chronopotentiometry and cell voltage variations during MG-Si electrorefining at various K_2SiF_6 concentrations in LiF-KF-5wt%K_2SiF_6 system to charge current density with 40mA/cm^2 for 5 hour at 800°C

In order to compare the electrochemical behavior of silicon according to the concentration of K_2SiF_6, two different concentrations, 30 wt% and 50 wt%, were tested for theoretically recovering 2.6 g of silicon at the cathode current densities of 83.3, 166.7, and 416.7 mA/cm^2 for 10 hr, 5 hr and 2 hr. Fig. 5 (a) shows the chronopotentiometry obtained with 30 wt% of K_2SiF_6 according to applied current density. The cathode potential was maintained at around 0.05 V (vs. Pt) regardless of the current density, whereas the anode potential increased from 0.2 to 0.3 and 0.5 (vs. Pt) as the applied current density increased from 83.8 to 166.7 and 416 mA/cm^2, respectively. Hence, the cell voltages mainly depend on the anode potentials as shown in Fig. 5 (b) because the cathode potentials were kept almost constant. Figure 5 (c) shows the
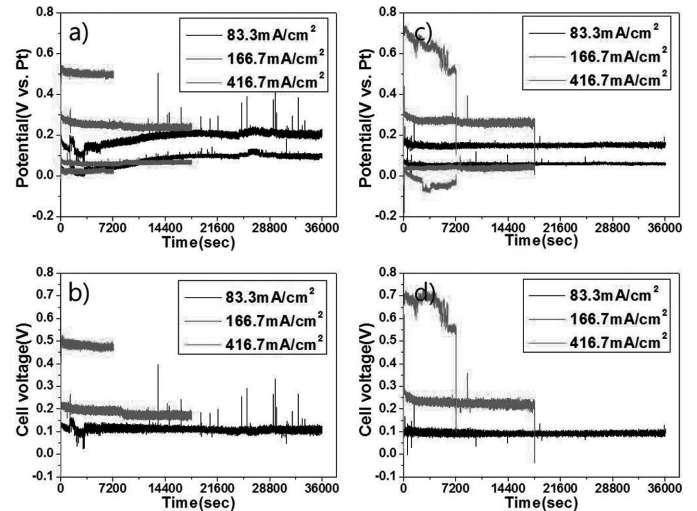

Fig. 5. (a)Chronopotentiometry and (b)cell voltage variations during MG-Si electrorefining at various K_2SiF_6 concentrations in LiF-KF-30wt% K_2SiF_6 system ;and (c) Chronopotentiometry and (d)cell voltage in LiF-KF-50wt% K_2SiF_6 system at 800°C

chronopotentiometry in a 50 wt% K_2SiF_6 electrolyte system at 800°C. Most of the current-potential responses were identical to that of the 30 wt% K_2SiF_6 electrolyte system except at 416.7 mA/cm^2 of applied current density. The anode potentials were 0.2 V (vs. Pt) and 0.3 V (vs. Pt) for 83.8 mA/cm^2 and 166.7 mA/cm^2 of applied current density, respectively,

and the cathode potential was 0.05 V for both cases. At a current density of 416.7 mA/cm^2 the anode and cathode potentials severely fluctuated throughout the electrorefining process and they approached 0 V (vs. Pt) and 0.7 V (vs. Pt) for the cathode and anode, respectively. The cell voltage variation mainly depended on the anode potential as shown in Fig. 5 (d). Compared to the cell potential of 30 wt% of K$_2$SiF$_6$ concentration, a higher cell potential was induced and the tendency was more clearly observed at a higher applied current density. This means the anode dissolution rate controlled the whole electrochemical reaction because a high ionic concentration hindered the dissolution of the anode feedstock due to a decreasing concentration deviation between the anode and electrolyte.

3.3. Formation of silicon nanofiber deposit

In order to observe the effect of the concentration of silicon in the electrolyte, electrodeposition was performed with 5 wt% of K$_2$SiF$_6$ at a current density of 40 mA/cm^2 for 5 hrs. Fig. 6 (a) shows the appearance of the cathode deposit containing the solidified electrolyte. It can be seen that the cathode deposit consists of three distinctive layers with different colors as shown in Fig. 6 (b). The inside of the deposit (1) is black and a dark brown layer (2) is sandwiched between the black layer and the light brown surface layer (3). Silicon has different colors depending on the particle size, black for coarse particles and brown for fine particles, especially at a nano scale. It can be predicted that the changes in color on the cathode shows that coarse silicon is deposited on the surface of the silver cathode and its size is decreasing as the deposition proceeds. As the electrolyte composed of LiF-KF 5 wt% K$_2$SiF$_6$ is white in the solid state, this color implicitly exhibits the color of the silicon deposit. To investigate the morphology of the silicon deposit recovered from the different locations in Fig. 6 (b), SEM data is presented in Fig. 7. Figure 7 (a) shows the SEM image taken from the surface of the silver cathode indicated in location (1) of Fig. 6 (b). Several tens of micrometer size silicon rods with dendritic growth at the tip are the main product and a fine whisker is also visible. Figure 7 (b) shows nanofiber with a 500 nm diameter taken from the middle part as shown in Fig. 6. (b)-(2). Figure 7 (c) shows more fine nanofiber with a 100 nm diameter taken

from the surface of the cathode deposit shown in Fig. 6. (b)-(3), where the underneath of the nanofiber in Fig. 7 c) is undissolved LiF crystal. From the series of the microstructural structure of the cathode deposit of silicon, the shape and size of the deposit tends to change from coarse crystal silicon to a fine fibrous shape as deposition proceeds. As the conductivity of pure silicon is not comparable to metallic material, cell resistivity is supposed to be increased with an increasing the thickness of cathode deposit. This increase in resistivity affects the potential increase during electrodeposition; furthermore, the edge of the cathode plate plays the role of high electric field induction [13, 14]. From the chronopotentiometry data of the electrodeposition in LiF-KF 5 wt% K$_2$SiF$_6$, a potential increase is observed as shown in Fig. 8. The anode potential started from below 0.1 V (vs. Pt) and gradually increased as the electrorefining proceeded. It should be noted that there are severe fluctuations throughout the experiment especially after 22 hr, probably due to low conductivity of the silicon anode feed stock and the electrolyte itself with a low ionic concentration of silicon. The cathode potential also gradually increased while the cell voltage remained almost constant as electrorefining proceeded, which means that the anode and cathode potentials increased simultaneously. In this electrorefining condition, a low electric field should have
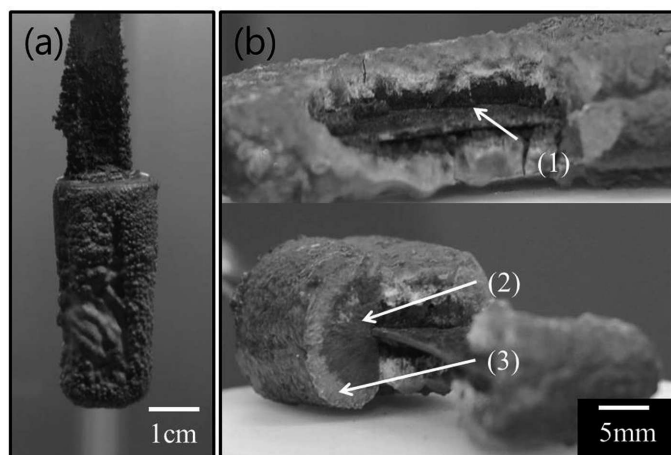

Fig. 6. (a) Cathode shape and (b) section image after electrorefining in LiF-KF-5wt% K$_2$SiF$_6$ system to charge current density with 40mA/cm^2 for 5 hour 800°
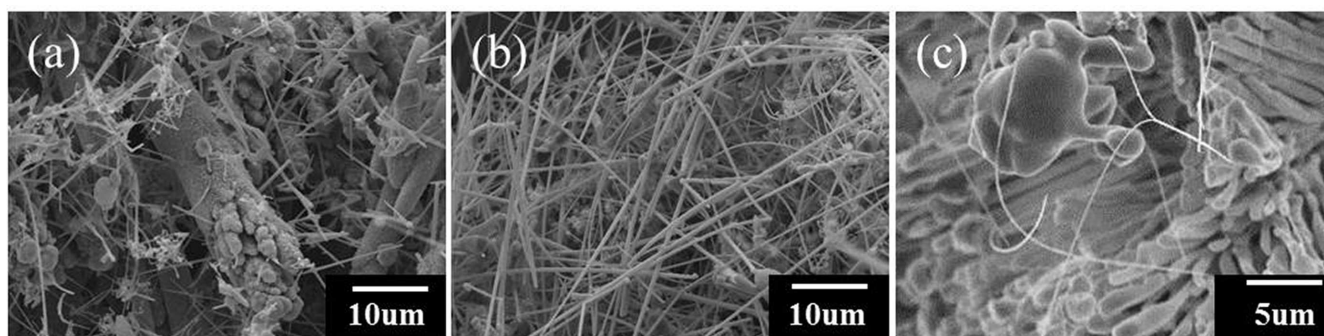

Fig. 7. Morphology of the cathode deposit according to location in LiF-KF-5wt% K$_2$SiF$_6$ system to charge current density with 40mA/cm^2 for 5 hour 800°C (a) plane part, (b) edge part, (c) certain distance part from the cathode

been induced on the electrodes as the low current density was applied. Hence, the deposition rate was also low under the low electric field leading to coarse dendritic growth of silicon on the silver electrode surface, while fine fibrous growth started as the electric field increased due to high resistance of the cathode deposit layer of the silicon [15]. A high resolution TEM image of silicon nano wire recovered by electrorefining with LiF-KF 5 wt% K_2SiF_6 at 800°C presented in Fig. 9. It has a diamond cubic crystal structure with a thickness of 15 nm. The surface is covered by a 1 nm oxide layer probably due to the oxidation during washing and handling out of the glove box. There are twin boundaries with (111) planes facing each other with 141°. The silicon nano wire grows in the direction of <11$\bar{1}$>.
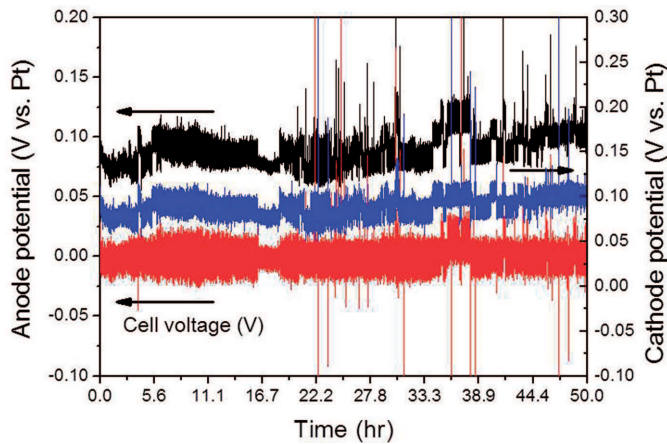

Fig. 8. Chronopotentiometry and cell voltage variations during MG-Si electrorefining in LiF-KF-5wt% K_2SiF_6 system with 16.7mA/cm^2 of current density for 50 hour at 800°C
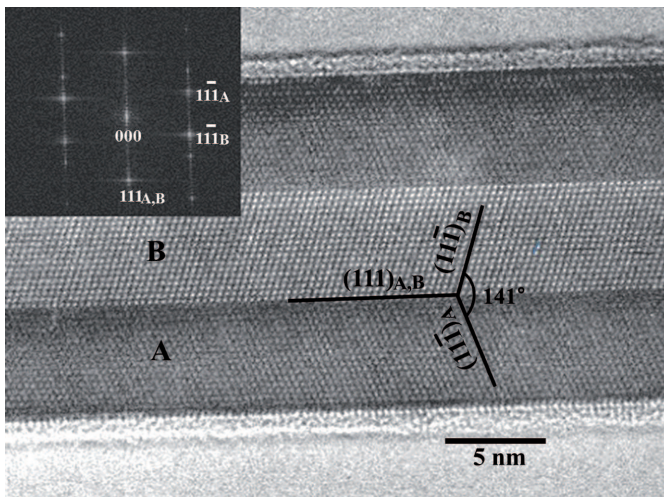

Fig. 9. High resolution TEM image of a silicon nanowire grown epitaxially

3.4. Coarsening of silicon deposit

To investigate the effect of ionic concentration of silicon, 30 wt% of K_2SiF_6 was introduced into the electrolyte, and the appearance of the cathode deposit is presented in Fig. 10. The color is completely different from that of the cathode deposit recovered at 5 wt% K_2SiF_6 with a brown color. The color of

the cathode deposit recovered at a high concentration of silicon is all black and the crystal size could be distinguished by bare eyes. The crystal size increased as the applied current density decreased when the K_2SiF_6 concentration was constant. With a constant applied current density of 83.3 mA/cm^2, coarse silicon crystal was observed at 30 wt% of K_2SiF_6 whereas coarser silicon crystal is observed at 50 wt% of K_2SiF_6 concentration for 166.7 mA/cm^2 and 416.7 mA/cm^2. It should be noted that a dense silicon coating layer was obtained at 16.7 mA/cm^2 of applied current density with 50 wt% K_2SiF_6 concentration.

The cathode deposit is supposed to include a lot of solidified electrolyte, so the recovered cathode deposits were washed with a 3 wt% HCl solution three times and dried, and then they were analyzed by XRD. The cathode deposit consisted of mainly silicon, and K_2SiF_6 was incorporated into the silicon product in several experimental conditions as shown in Fig. 11. It is interesting to see that the deposit recovered
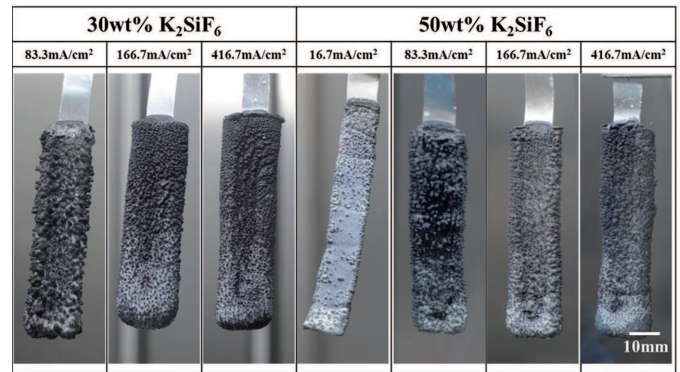

Fig. 10. Typical cathode shape change after electrorefining with respect to applied current density and concentration of K_2SiF_6
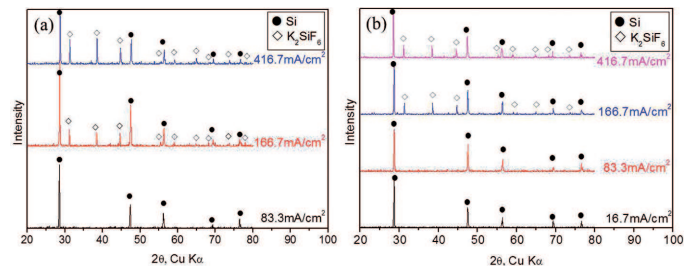

Fig. 11. XRD patterns of washed cathode deposit by 3% HCl solution for 3 times in LiF-KF (a)30wt% and (b)50wt% K_2SiF_6

at a higher current density of more than 166 mA/cm^2 have residual K_2SiF_6. At a 30 wt% K_2SiF_6 concentration, K_2SiF_6 peaks appeared at 416.7 mA/cm^2 and its fraction decreased as the current density decreased to 166.7 mA/cm^2. The residual K_2SiF_6 peaks completely disappeared at 83.3 mA/cm^2 of current density as shown in Fig. 11 a). Similar results were obtained with 50 wt% of K_2SiF_6 concentration as shown in Fig. 11 b). There are residual K_2SiF_6 peaks at 416.7 mA/cm^2 and 166.7 mA/cm^2 of applied current density and pure silicon peaks were obtained below 83.3 mA/cm^2 of applied current densities. These results show that there is a direct relation between the applied current density and incorporation of K_2SiF_6 in the cathode deposit. Since the K_2SiF_6 is not deposited at the cathode electrochemically,
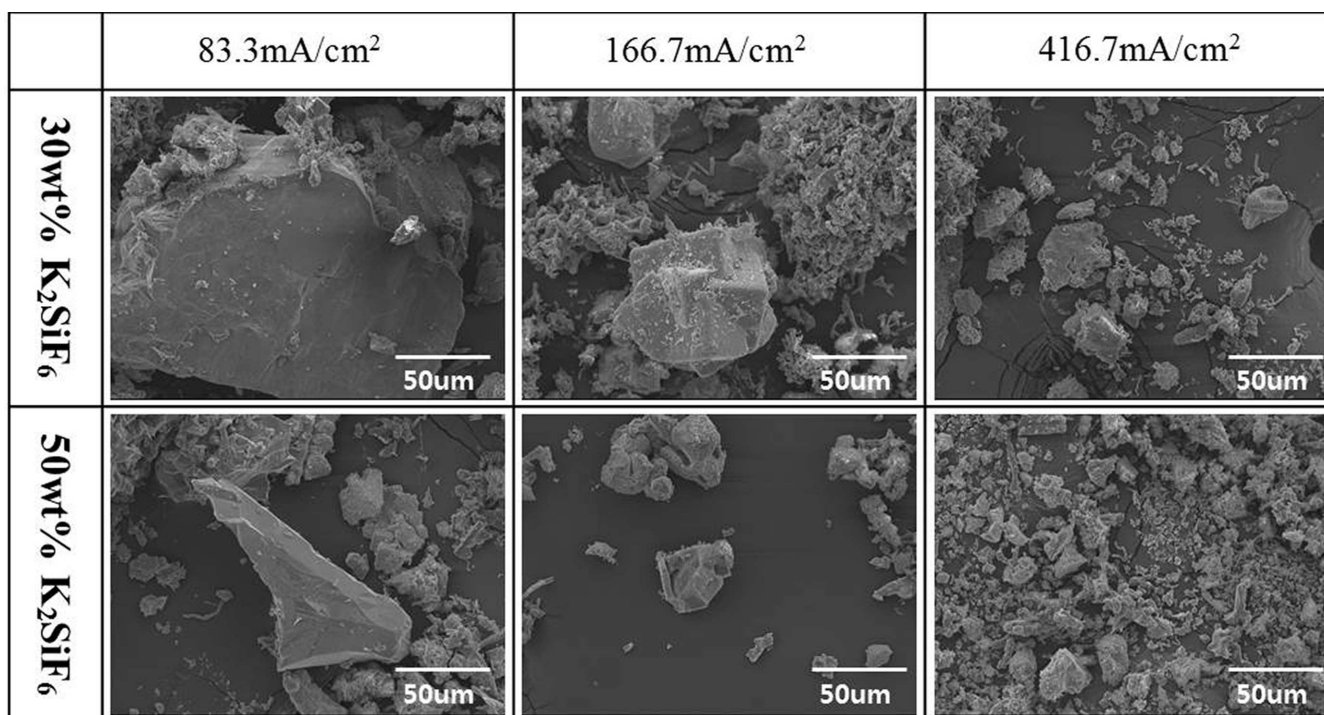
Fig. 12. Morphology change of cathode deposit with varying K_2SiF_6 concentrations in salt and applied current densities
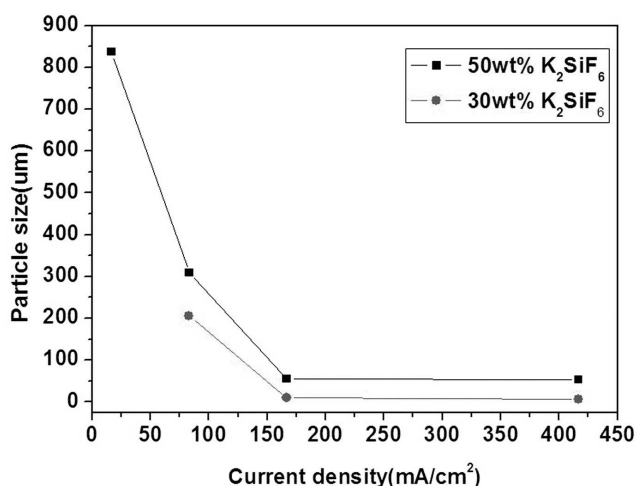

Fig. 13. Particle size of cathode deposit with varying K_2SiF_6 concentrations in salt and applied current densities

there is another reason for the contamination in the cathode deposit. In order to interpret this phenomena, the microstructure of the cathode deposit was observed by SEM as shown in Fig. 12. At a low current density of below 83.3 mA/cm^2, a coarse and dense silicon deposit was formed regardless of the concentration of K_2SiF_6 as shown in Fig. 12. When the current density increased to more than 166.7 mA/cm^2, the particle size decreased and a fine silicon powder was obtained at 416.7 mA/cm^2 of applied current density. It should be noted that no fibrous silicon deposit was observed in these electrodeposition conditions, but a granular type deposit was obtained with a high concentration of K_2SiF_6. When a deposit was formed at the cathode, molten salt was also incorporated into the deposit, and the amount of adhering salt depended on the porosity in the deposit. As confirmed by SEM data in Fig. 2, a dense granule was formed under a low current

density while fine powder was obtained with a high current density. We believe that molten salt was captured in the pores during the growth of the silicon. The particle size variation with K_2SiF_6 concentration is depicted in Fig. 13. As expected, largest particle size, 850 μm, was obtained with 50 wt% of K_2SiF_6 concentration under 16.7 mA/cm^2 of current density and the particle size decreased with an increasing current density. The tendency of 30 wt% of K_2SiF_6 was very similar to that of 50 wt% of K_2SiF_6 but the level particle size slightly decreased. There was no change in the particle size when the current density was more than 166.7 mA/cm^2.

4. Conclusion

An electrodeposition experiment was conducted to obtain silicon with high purity from MG-Si, which has a lower purity. The applied current density and concentration of K_2SiF_6 are important parameters affecting the size and shape of a silicon deposit. Particle size decreased with an increasing applied current density regardless of the concentration of K_2SiF_6. When the concentration of K_2SiF_6 decreased below 5 wt%, silicon nano fiber was obtained and its size and shape varied according to the location on the silver cathode plate. The morphology characteristic of the prepared silicon nano fiber was analyzed by high resolution TEM and showed twin boundaries with a 141° angle between (111) planes.

REFERENCES

[1] C.K. Chan, H. Peng, G. Liu, K. McIlwrath, X.F. Zhang, R.A. Huggins, Y. Cui, Nat. Nanotechnol. **3**, 31 (2008).

[2] T.D. Bogart, A.M. Chockla, B.A. Korgel, Curr. Opin. Chem. Eng. **2**, 286 (2013).

[3] M. Ge, J. Rong, X. Fang, C. Zhou, Nano Lett. **12**, 2318 (2012).

[4] D.J. Lee, H. Lee, M.H. Ryou, G.B. Han, J.N. Lee, J. Song, J. Choi, K.Y. Cho, Y.M. Lee, J.K. Park, ACS Appl. Mater. Interfaces **5**, 12005 (2013).

[5] H.Y. Ryu, Y.S. An, B.Y. Jang, J.S. Lee, H.H. Nersisyan, M.H. Han, J.S. Noh, J.H. Lee, Mater. Chem. Phys. **137**, 160 (2012).

[6] J.H. Lee, K.H. Oh, Y.H. Kang, S.C. Hwang, H.S. Lee, J.B. Shim, E.H. Kim, S.W. Park, Nucl. Technol. **165**, 370 (2009).

[7] K.T. Park, T.H. Lee, N.C. Jo, H.H. Nersisyan, B.S. Chun, H.H. Lee, J.H. Lee, J. Nucl. Mater. **436**, 130 (2013).

[8] M.S. Islam, M.A. Rhamdhani, G.A. Brooks, Solar-grade silicon: current and alternative production routes, Proceedings of 'Engineering a Better World', the Chemeca 2011 Conference, Sydney, Australia, 2011 (http://www. conference.net.au/chemeca2011/papers/448.pdf).

[9] R. Boen, J. Bouteillon, J. Appl. Electrochem. **13**, 277 (1983).

[10] K.L. Carleton, J.M. Olson, A. Kibbler, J. Electrochem. Soc. **130**, 782 (1983).

[11] G.J. Kipouros, S.N. Flengas, J. Electrochem. Soc. **132**, 1087 (1985).

[12] J. Sangster, J. Phase Equilib. Diffus. **27**, 190 (2006).

[13] S.H. Kim, S.B. Park, S.J. Lee, J.G. Kim, H.S. Lee, J.H. Lee, Nucl. Eng. Des. **257**, 12 (2013).

[14] R. Bansevicius, J.A. Virbalis, J. Electrostat. **64**, 226 (2006).

[15] Y. Shibuta, T. Sato, T. Suzuki, H. Ohta, M. Kurata, J. Nucl. Mater. **436**, 61 (2013).